

Integrated Magneto-photonic Non-Volatile Multi-Bit Memory

Hamed Pezeshki^{1,2*}, Pingzhi Li¹, Reinoud Lavrijsen^{1,2}, Martijn Heck² and Bert Koopmans^{1,2}

¹Department of Applied Physics and Science Education, Eindhoven University of Technology, Eindhoven, 5612 AZ, Netherlands.

²Eindhoven Hendrik Casimir Institute, Center for Photonic Integration, Eindhoven University of Technology, Eindhoven, 5600 MB, Netherlands.

*Corresponding author(s). E-mail(s): h.pezeshki@tue.nl;

Abstract

We present an integrated magneto-photonic device for all-optical switching of non-volatile multi-bit spintronic memory. The bits are based on stand-alone magneto-tunnel junctions which are perpendicularly magnetized with all-optically switchable free layers, coupled onto photonic crystal nanobeam cavities on an indium phosphide based platform. This device enables switching of the magnetization state of the bits by locally increasing the power absorption of light at resonance with the cavity. We design an add/drop network of cavities to grant random access to multiple bits via a wavelength-division multiplexing scheme. Based on a three-dimensional finite-difference time-domain method, we numerically illustrate a compact device capable of switching and accessing 8 bits in different cavities with a 5 nm wavelength spacing in the conventional (C) telecommunication band. Our multi-bit device holds promise as a new paradigm for developing an ultrafast photonically-addressable spintronic memory and may also empower novel opportunities for photonically-driven spintronic-based neuromorphic computing.

1 Introduction

Nowadays, there is no doubt on the critical role of integrated photonics in telecommunications for achieving ultrafast, and energy-efficient on-chip and inter-chip data transmission [1–3]. Moreover, there has been tremendous progress in novel application perspectives, such as in optical neural network computing and quantum information processing [4–6]. As for the power and delay overhead related to data transportation [5, 7, 8], encoding information as optical bit patterns in the photonic domain without any opto-electronic conversion steps can be beneficial from the perspectives of modulation speed, power consumption, data transfer bandwidth, and cross talk. An important aspect of integrated photonics to extend its application perspectives relies on the implementation of photonic memories [9]. Using these, versatile functionalities in signal processing, such as buffering and filtering [10, 11], optical computing [12, 13], data storage [14, 15], and quantum information [16] can be realized.

Photonic memories are typically implemented in several ways. For optical buffers in signal processing [10, 11], microring resonators and delay lines are used to temporarily store the optical signals before their degradation. In view of the very large variation in the rate of incoming data, excessive area and energy overhead are required. Recently, non-volatile memories such as phase-change materials (PCMs) and nonlinear optical materials, whose optical and electrical properties change upon optical and electrical stimuli [17–22], are being considered as an alternative due to their much longer retention time, lower power consumption, higher optical contrast, and fast switching speed [4, 6, 21, 22]. Nonetheless, PCM-based memories would require large transient power and slow writing time in the range of nanoseconds for switching only a single bit due to the intrinsic atomic dynamics [15, 23]. Addressing multiple bits using these memories would lead to devices with very large footprints [24, 25] due to the use of several microring resonators.

In some more recent demonstrations, it was shown that some material platforms based on spintronics can be all-optically switched (AOS) and read (AOR) [26–28]. The random access memory based on a spintronic material platform (termed as MRAM) is by definition much faster and energy efficient than other novel memory types including PCM-based ones. The characteristic differences are rooted in the much faster and energy efficient spin dynamics [29] compared to phase change processes. Moreover, it has been shown that AOS of spintronic materials can be completed in the order of picoseconds with high energy efficiency [30]. Introducing spintronic material based devices would not only enlarge the library of photonic memories, but also extend the functionalities of the entire platform by hybridizing it with integrated spintronics. Such a concept has comprehensively been investigated based on both alloys and the layered cobalt and gadolinium (Co and Gd) material system, showcasing AOS using optical pulses with incident energies in the range of femtojoule (fJ) [31–34].

Recently, Becker *et al.* [35] proposed a building block for spintronic photonic integration for accessing magneto-tunnel junctions (MTJs) by vertically

projecting light onto them using a two-dimensional grating coupler. However, such an approach comes with a large footprint and diffraction limit drawbacks. Then, Pezeshki *et al.* [36, 37] proposed a hybrid plasmonic-photonic device for integrating spintronic racetrack memory with a photonic waveguide to access nanoscale ferrimagnet bits by injecting fJ (sub) picoseconds light pulses through the waveguide. Nonetheless, as Kimel and Li [30] stated, incorporating magneto-photonic devices such as opto-MTJs [38] in MRAM data storage applications necessitates a large-scale integration of MTJ building blocks, randomly accessible at will for AOS and AOR. Kimel and Li addressed the issue of selective accessibility by proposing time-division and wavelength-division multiplexing schemes (TDM and WDM) [30]. The TDM is a time-domain optical approach in telecommunications, where a number of optical signals are periodically interleaved in time, transmitted together, and then separated according to different arrival times. In contrast, the WDM technique is a frequency (wavelength)-domain optical approach in which optical signals with different wavelengths are combined, transmitted, and later separated based on their wavelengths. They suggested a method exploiting a cross-bar array of optical waveguide-based Bragg grating resonators for the purpose of TDM and WDM [30]. Although an interesting proposal, their proposed far-field method comes with large footprint, low out-coupling efficiency, inefficacy from the power consumption aspect and according to the authors, their WDM scheme requires lots of lasers at different wavelengths.

In this paper, we propose, and numerically explore an energy-efficient device functioning based on a near-field WDM approach through the use of a compact add/drop network [39] of photonic crystal (PhC) [40, 41] nanobeam cavities on the indium phosphide (InP) membrane on silicon (IMOS) platform. In our device, each MTJ with a diameter of 60 nm acts as 1 bit, and is coupled onto the center of an individual PhC cavity with a distinct resonance wavelength. Using a three-dimensional finite-difference time-domain (FDTD) method, Lumerical FDTD [42], we numerically demonstrate that by changing the wavelength of incident light, our device can enable wavelength-dependent switching of at least 8 bits, located at different cavities with a 5 nm wavelength spacing. The device concept is generic and can be implemented in other major photonic platforms such as silicon photonics (SiPh) [43, 44] and silicon nitride (SiN) [45, 46] photonics. Our proposed approach makes a step forward towards spintronic-photonic integration, providing with ways to energy-efficient and fast access to spatially separated MRAM devices.

2 Device design

2.1 Device layout

In this work, we propose a device design for multi-bit spintronic memory based on an add/drop network, which is shown schematically in Fig. 1. As sketched, it involves a photonic bus line, laterally placed between two photonic drop lines. The bus line is a meandering InP waveguide for carrying optical incident

light within the network. The drop lines consist of InP nanobeam PhC cavities, i.e., grating-based cavities, C_1 to C_8 , each of which having one resonance wavelength and resonating at a particular wavelength, required for our WDM scheme. A cylindrical MTJ is evanescently coupled at the center of each cavity with a unique resonance wavelength (in Fig. 1 represented by a distinct color). Each MTJ consists of two ferromagnetic layers of a top pinned reference layer and an AOS-enabled free layer stacked to each other via a non-magnetic insulating metal oxide tunneling barrier (refer to [38] for more information). The free layer in our work is considered based on the Co/Gd material system, a (3d) transition metal and a (4f) rare-earth ferromagnet essential for AOS [30, 31, 47], whose threshold fluence has been priorly characterized [34, 48]. The device works with in-coupling a picosecond optical Gaussian pulse into a fundamental transverse electric (TE_0) mode of the bus waveguide. As the TE_0 mode propagates through the waveguide, depending on the wavelength of the incident pulse, the pulse energy is transferred only to the designated cavity upon fulfilment of resonance conditions. Upon resonance in a cavity, the localized field enhancement by the cavity increases the amount of power absorbed in the coupled MTJ, leading to its ultrafast toggle-AOS upon fulfilling the required fluence threshold [32, 37, 48, 49]. The subsequent switching is sensed by the tunneling magnetoresistance (TMR) effect, as the relative alignment of the magnetization between the free layer and the pinned top layer is changed. It is worth mentioning that MTJs are electrical devices requiring bottom and top electrodes, where the bottom electrodes are very thin films, less than 10 nm, of transparent indium tin oxide [38, 50] in order to allow the light passage. This thin film contributes negligibly to the design and performance characteristics but complicates the modelling and discussion. So, for the sake of simplicity without losing generality, these electrodes are neglected, inspired by the work of Chen *et al.* [50].

In order to design a multi-bit device using the proposed WDM scheme, there are two important design steps that need to be considered for having a desired device performance, which will be further elaborated on in the rest of this section.

2.2 Design criteria

We consider an add/drop network of 8 cavities tuned to various wavelengths across the telecommunication C-band to all-optically switch an MTJ depending on the wavelength of the incident light. The challenge is to switch each bit independently without unintended switching of any other MTJs. We first need to provide enough energy for switching the entire bit, which is called the saturation energy U_{sat} . We need to ensure that the minimum pulse energy, U_{min} , fed to the device for successful switching of the targeted bit in the cavity C_j tuned to its resonance wavelength, λ_j , must be equal or above the saturation energy, i.e. $U_{\text{min}}[j] \geq U_{\text{sat}}[j]$. The pulse energy may off-resonantly be coupled to undesigned cavities due to cross talk. It is then equally important to guarantee that the switching will not occur at any other cavities $k \neq j$ for each

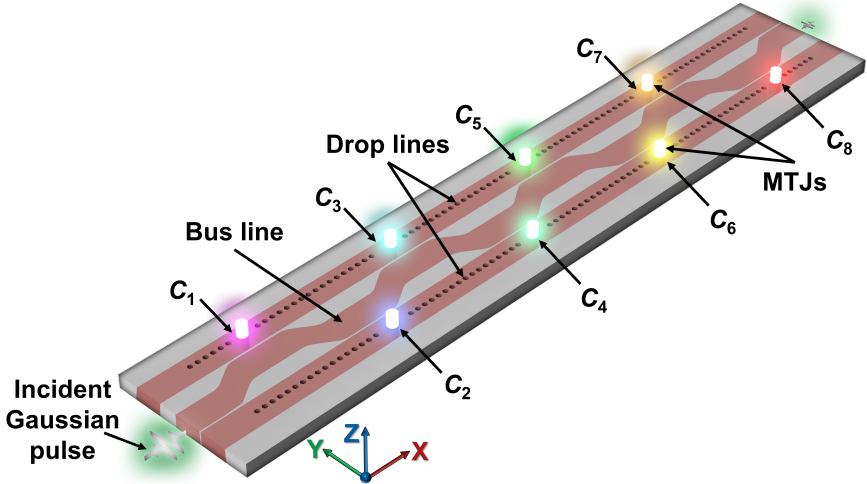


Fig. 1 Conceptual illustration of the device design as a building block for multi-bit spintronic memory. The device is an add/drop network of 8 spatially separated nanobeam photonic crystal (PhC) cavities to randomly access magnetic bits presented by opto magnetic-tunnel junctions (MTJs). The cavities are denoted as C_1 to C_8 . Different colors enlightening the cavities showcase the monotonic change of the resonance wavelength for illustration purposes, which should not be confused with the realistic wavelengths within the telecommunication C-band, which are separated by 5 nm in this work. The dimensions are not in scale for the sake of clarity.

λ_j due to cross talk. In other words, the amount of the pulse energy in any unwanted cavity should be kept less than the threshold energy, U_{th} , for which at least a fraction of the bit is switched. Thus, the maximum energy limit for switching the bit j , $U_{\text{max}}[j]$, without unwanted switching of other bits k should be less than $U_{\text{th}}[k]$. Hence, the goal is to find the range of the incident pulse energy fulfilling the above-mentioned two criteria. Without loss of generality, we suppose that the full-width at half-maximum (FWHM) of each resonance cavity (Γ), the wavelength spacing between each subsequent cavities, the total absorption loss by each cavity (L) and MTJs (A) are identical. Therefore, saturation, U_{sat} , and threshold energies, U_{th} , of MTJs will be identical.

The absorption loss profile of the cavities is obtained by fitting based on a Lorentzian function as follows:

$$L(\lambda_0, \lambda_r, \Gamma) = \frac{L_0 \Gamma^2}{(\lambda_0 - \lambda_r)^2 + \Gamma^2}, \quad (1)$$

where L_0 is the absorption loss by the cavity at resonance, λ_0 and λ_r are the incident and resonance wavelengths, respectively. According to the first criterion and considering cross talk contributed by cavities upstream the network, the minimum pulse energy for successfully switching the bit j , $U_{\text{min}}[j]$, can be obtained from:

$$U_{\min}[j] \left(\prod_{i=1}^{j-1} (1 - L[i, j]) \right) L[j, j] A[j, j] \geq U_{\text{sat}}[j] \quad \forall j = 1 \cdots 8, \quad (2)$$

where $L[i, j]$ is the absorption loss contributed by the upstream cavity i , when the incident wavelength is tuned to the resonance wavelength of the C_j cavity, i.e. λ_j . The $L[j, j]$ and $A[j, j]$ are the C_j cavity's absorption loss and the fraction of the absorption loss in that cavity which is used to perform AOS on the target bit j , respectively. Note that the reflection off the designed cavity is so small that the possible interference between reflected light off the cavity and light in the bus waveguide can be neglected. Based on the second criterion, the incident pulse energy at λ_j should be low enough such that the energy deposition at the C_k cavity is lower than the threshold energy $U_{\text{th}}[k]$, required for switching at least a part of the area of any other bit $k \neq j$. Thus, there is an upper limit for the incident pulse energy, $U_{\max}[j, k]$, which can be calculated as following:

$$U_{\max}[j, k] \left(\prod_{i=1}^{k-1} (1 - L[i, j]) \right) L[k, j] A[k, j] < U_{\text{th}}[k] \quad \forall k \neq j = 1 \cdots 8, \quad (3)$$

where $L[k, j]$ and $A[k, j]$ are the C_k cavity's absorption loss and the fraction of the absorption loss in that cavity for the incident pulse energy at λ_j , respectively.

2.3 Implementation of design criteria

In order to demonstrate the design criteria, we emphasize more specifically the two essential parameters of a resonance cavity, that is the resonance width, Γ , and efficiency. We apply the above-mentioned concepts to an analytical energy absorption analysis of four typical cases: a non-working device, a conditionally-working device, a working device, and a device with less efficient resonance cavities. To do so, as a concrete example, we consider $L_0 = 0.5$, that is an initial absorption loss of 50% by cavities at resonance, $A = 1$, that is 100% of the loss being absorbed by the magnetic bit, $U_{\text{sat}} = 1$ as a normalization, and $U_{\text{th}} = 0.9$, i.e. 90% of U_{sat} , motivated by the fact that the light absorption is non-uniform in an MTJ (see [37] for more insight). We further chose the incident wavelengths from the C-band with a 5 nm spacing. Note that as of here, we will specify "threshold" pulse energies as the fraction of U_{sat} in dimensionless units.

2.3.1 Non-working case

We first argue the decisive role of the narrow resonance width of a cavity by assuming a non-working case, for which we consider cavities with a broad resonance spectrum, for instance with $\Gamma = 30$ nm. We plotted U_{\min} and U_{\max}

as defined in Eqs. 2 and 3 in Fig. 2 (a) for this case. In this figure, the minimum energy required to switch the targeted bit in the cavity C_j at $\lambda_r[j]$ for $j = 1$ to 8, U_{\min} , is indicated by the solid purple line. The dashed and dotted lines represent the upper limit of the energy required for switching the targeted bit in C_j , $U_{\max}[j, k]$, without unwanted switching of all other bits $k \neq j$, i.e., $U_{\max}[j, k] > U_{\min}[j]$ for all $k \neq j$. From this point onward, we neglect the index $[k]$ for U_{\max} , e.g. $U_{\max}[j = 1, k]$ is denoted as $U_{\max}[1]$ for simplicity. According to Fig. 2 (a), by going downstream, U_{\min} increases because of the absorption loss in the earlier cavity/cavities in the chain. Based on this plot, at the C_1 cavity, when using its resonance wavelength for switching the bit, very high energies are required to switch other bits in the C_2 to C_8 cavities, as they are off-resonant and also further downstream. In contrast, we need a higher energy for switching the targeted bit at the C_8 cavity, i.e. > 43 , which exceeds the essential energy level for switching the bits in other cavities, i.e. ≤ 20 , as highlighted by a red-dotted ellipse in Fig. 2 (a). In this case, by switching the bit in the C_8 cavity, other bits further upstream get switched-on erroneously by the energy leakage due to cross talk. Thus, in this case, at least one bit will be inadvertently switched together with the targeted bit.

2.3.2 Conditionally-working case

For the second case, by reducing the resonance width from $\Gamma = 30$ nm to $\Gamma = 6$ nm, we can have a device that conditionally works. The result for this case is shown in Fig. 2 (b). In contrast to the case in Fig. 2 (a), the U_{\min} limit required to switch the target bit in the cavity C_j at $\lambda_r[j]$ for $j = 1$ to 8 is below the U_{\max} limit needed for unwanted switching of the bits $k \neq j$. Even though $U_{\min} < U_{\max}$, there is only a marginal difference for cavity numbers $j > 1$. Besides, $U_{\min}[j = 8] > U_{\max}[j = 2, k = 1]$ and $U_{\max}[j = 3, k = 2]$ as highlighted by a red-dotted ellipse. This means that, for instance, by applying a fixed input pulse energy of $U_{\min}[j = 8]$ for switching the bits in the C_2 and C_3 cavities, we suffer from unwanted switching of the bits in the C_1 and C_2 cavities, respectively. In other words, the device can only be made to work by choosing dynamically lower pulse energy for switching the targeted bits upstream. We need a higher energy to switch the bit in the C_8 cavity (without unwanted switching elsewhere upstream), and a lower one when targeting the bit in the C_2 and C_3 ones. This requirement will lead to a less trivial operational scheme in the sense that laser energy must be tuned carefully at each different wavelength.

2.3.3 Unconditionally-Working case

Our analysis shows that the cavities with a resonance width of $\Gamma < 4$ nm make the device work unconditionally. We introduce such a working device by choosing $\Gamma = 3$ nm, where the result is shown in Fig. 2 (c). Based on this plot, the U_{\min} limit is well below all the U_{\max} limits, i.e. less than the threshold energies of all other bits in the off-resonant cavities. For a pulse energy between ~ 3 and ~ 7 as depicted by a red double-headed arrow, we only have events

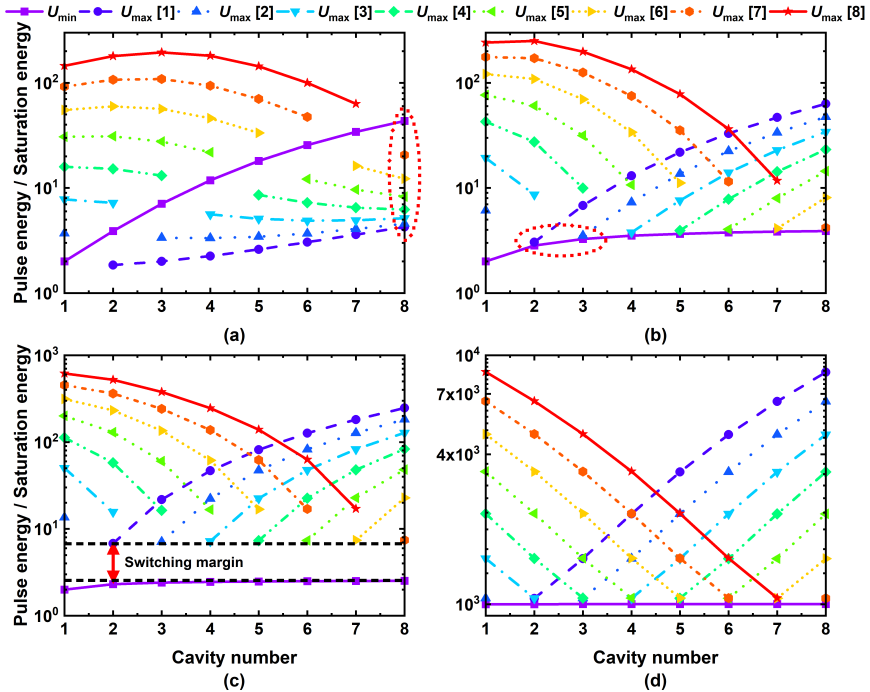


Fig. 2 Design considerations. Implementing the design criteria for four major cases of: (a) a non-working device with full-width at half-maximum (FWHM) of $\Gamma = 30$ nm, (b) a device with $\Gamma = 6$ nm that conditionally works, (c) a working device with $\Gamma = 3$ nm, and finally (d) a device with less efficient resonance cavities with $L_0 = 0.001$ for $\Gamma = 12$ nm. The L_0 in (a-c) is 0.5. Note that for the sake of simplicity, we neglected the index $[k]$ for U_{\max} , e.g. $U_{\max}[j = 1, k]$ is $U_{\max} [1]$.

of desired switching of the targeted bits, without falsely switching of other bits. Overall, there is a significant energy margin between the U_{\max} and U_{\min} , which makes it possible to address all the bits in the cavities using the same laser energy, $U_{\min}[j] = \text{const.}$ for all $j = 1 - 8$.

2.3.4 Less efficient cavity case

Finally, for the last case, we demonstrate the role of the efficiency of the cavity by considering a device with much less efficient resonance cavities. To model such a device, we set $L_0 = 0.001$, 0.1 % of the incident power is coupled to each cavity at its resonance. We show the result of an extreme case in which $\Gamma = 12$ nm in Fig. 2 (d). Based on this plot, we can see U_{\min} for switching downstream and upstream bits is almost equal and is below all the U_{\max} limits because of poor coupling condition between the bus and drop lines in the add/drop network. More importantly, this case unravels the inverse relation between the energy efficiency of switching and performance of resonance cavities. Here, correct switching of the bits in cavities with much wider Γ can become possible

but at the expense of much higher pulse energies compared to the conditionally-working and working cases. Altogether, the results of this analytical study serve as a general guideline for designing our multi-bit spintronic memory.

3 Results

To address 8 magnetic bits across the C-band using our proposed add/drop scheme, we should consider a case of a realistic device. For this purpose, we used a cavity which is formed via removing three holes across the axis of a 1D PhC lattice, known as L3 cavity [51]. Figure 3a shows a schematic of this cavity loaded with an MTJ possessing a radius of $r_m = 30$ nm (see Fig. 3b), where the waveguides' width and height are $w = 570$ nm and $h = 280$ nm respectively, and the gap between the bus line and drop lines around the coupling area is $g = 200$ nm. We designed and optimized 8 different PhC cavities, with a lattice constant and a hole radius of $a = 370$ nm and $r = 85$ nm (see Fig. 3b), without the coupled MTJs to resonate across the wavelength range of 1535 to 1570 nm, considering the wavelength spacing of 5 nm achieved by modifying the size, $2r_d$, and/or position, x_d , of the point defects in purple at the right and left sides of the cavity (see Fig. 3b). Table 1 shows the cavities' design parameters and resonance properties based on their normalized electric field resonance spectra, probed in the middle of the waveguide and at the center of the cavity, as shown in Figs. 3c and 3d at two conditions of without(unloaded) and with (loaded) the coupled MTJs. This table shows that the Γ of unloaded cavities varies between 2.45 nm at $\lambda_r = 1570$ nm and 4.9 nm at $\lambda_r = 1535$ nm. On the contrary, the loaded cavities have slightly broader resonance spectra, $\Gamma = 3.23$ nm at $\lambda_r = 1570$ nm and $\Gamma = 7.5$ nm at $\lambda_r = 1535$ nm, due to the absorption losses imposed by the coupled MTJs.

To further illustrate the wavelength-selectivity of the device loaded with MTJs, the electric field distribution across the section surrounding the C_4

Table 1: Design parameters and resonance properties of the cavities for the use in the add/drop network.

Cavity number	r_d^1 (nm)	x_d^1 (nm)	λ_{ru}^2 (nm)	Γ_{ru}^2 (nm)	λ_{rl}^2 (nm)	Γ_{rl}^2 (nm)
C ₁	103.5	18.5	1535	4.90	1533	7.50
C ₂	103.5	29.6	1540	4.00	1538	6.00
C ₃	103.5	38.5	1545	3.50	1543	5.25
C ₄	85	27.4	1550	2.90	1548	4.65
C ₅	85	34.8	1555	2.75	1553	4.20
C ₆	66.5	34.8	1560	2.50	1558	3.60
C ₇	61	46.3	1565	2.50	1563	3.58
C ₈	66.5	27.4	1570	2.45	1568	3.23

¹ The parameters r_d and x_d stand for the size of the point defects and the spatial shift in their position.

² $\lambda_{ru(rl)}$, and $\Gamma_{u(l)}$ indicate the resonance wavelength and full-width at half-maximum of the corresponding cavities in two cases of unloaded and loaded, respectively.

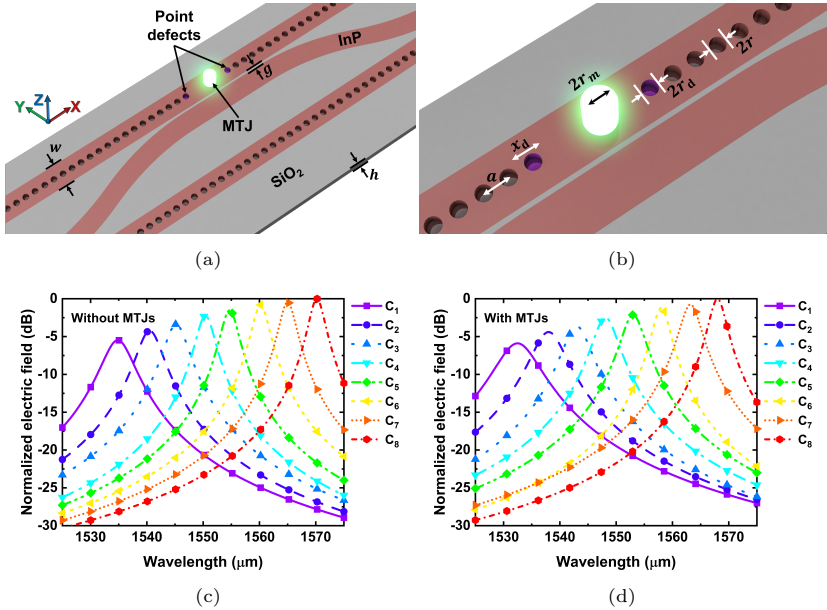


Fig. 3 Design and response of the cavities for the purpose of multi-bit spintronic memory. (a) A generic schematic of a L3 cavity loaded with an MTJ, where the waveguide’s width and height are $w = 570$ nm and $h = 280$ nm, and the gap between the bus line and drop lines around the coupling area is $g = 200$ nm. (b) The magnified view of the L3 cavity in which the PhC cavity’s lattice constant and holes radii are $a = 370$ nm and $r = 85$ nm, respectively. The point defects of the cavity are shown in purple, where their radius and the spatial shift in their position are denoted by r_d and x_d . The coupled MTJ is also shown in greenish glow color with the radius of $r_m = 30$ nm. (c, d) Normalized electric field resonance spectra of the designed cavities probed in the middle of the waveguide and at the center of the cavity for the two cases of without and with the coupled MTJs.

cavity at its resonance wavelength $\lambda_{r1} = 1548$ nm as well as the resonance wavelengths of its neighboring cavities C_3 and C_5 , i.e. 1543 and 1553 nm, are presented in Fig. 4. Based on Figs. 4a and 4c, at $\lambda_0 = 1543$ and 1553 nm, the coupling to C_4 is very weak and the incident light mostly propagates through the waveguide. However, the light coupling to C_4 becomes intensified at $\lambda_0 = 1548$ nm as shown in Fig. 4b, for which the cavity provides $> 3\times$ electric field enhancement relative to the off-resonant cases. It can be seen that by de-tuning the wavelength of the incident light by ± 5 nm, we cannot excite C_4 due to the weak coupling between the bus and drop lines.

All-optical switching of magnetization is induced by fast non-adiabatic heating [31, 47] and a discrete, pulse length dependent threshold energy density. Hence, we evaluate the energy efficiency of AOS in our FDTD simulations based on the instant absorbed energy density in the coupled MTJs [37]. In

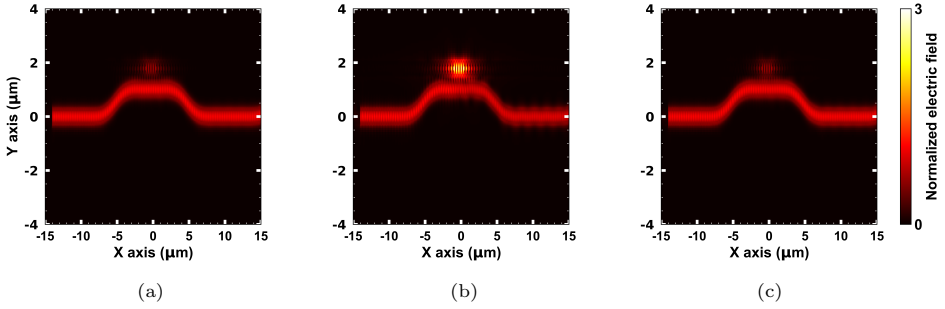


Fig. 4 Dependency of the cavity response on the wavelength. (a - c) Electric field distribution across the C_4 section for the incident light wavelengths of 1543, 1548, and 1553 nm, respectively.

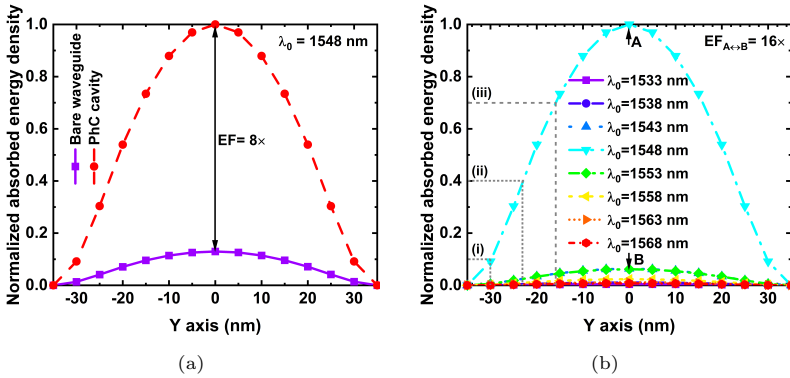


Fig. 5 Absorbed energy density distribution across MTJ. Normalized absorbed energy density along the Y axis cut-through the middle of the cobalt (Co) layer, integrated across the MTJ’s surface in direction of the X axis (refer to Fig. 3 for X and Y axes definitions.) for: (a) bare waveguide and the PhC cavity C_4 at $\lambda_0 = 1548$ nm, and (b) the C_4 cavity for the incident light wavelengths from $\lambda_0 = 1533$ to $\lambda_0 = 1568$ nm, respectively. “EF” stands for enhancement factor and “A” and “B” point to the peak of the absorbed energy density curves at $\lambda_0 = 1548$ nm and $\lambda_0 = 1548 \pm 5$ nm, respectively. The three points indicated by (i), (ii), (iii) indicate the cases of non-working, marginally-working, and unconditionally-working devices, respectively.

our simulation, we extract the spatial distribution of the absorbed energy density by the magnetic switching layer, i.e. Co/Gd (represented by a Co layer instead in our simulation). Figure 5a shows the one-dimensional distribution of the absorbed energy density cut-through the middle of the Co layer of the MTJ in C_4 for the two devices of the bare waveguide and the proposed PhC device. The results are shown along the Y axis, which are integrated across the MTJ’s surface along the X axis (refer to Fig. 3 for X and Y axes definitions.)

and normalized to the maximum absorbed energy. As shown, the C_4 cavity at its resonance, i.e. $\lambda_0 = 1548$ nm shows an $8\times$ peak-to-peak enhancement in the absorbed energy density by the MTJ. In our previous work [37], we theoretically showed that with a $7\times$ enhancement in the absorbed energy density, we can exceed the absorbed switching threshold of 0.5 mJ/cm² [33, 37] for an incident pulse energy of only 0.6 pJ without running into the regime of nonlinear absorption. Therefore, it can be seen that the proposed cavity can provide the condition for AOS.

We have further illustrated the absorbed energy distribution across the MTJ at the C_4 as a function of the wavelength of incident light, from $\lambda_0 = 1533$ to $\lambda_0 = 1568$ nm, in Fig. 5b. According to this figure, the absorbed energy density is maximum for $\lambda_0 = 1548$ nm, which is equal to the resonance wavelength of the loaded cavity C_4 . Changing the wavelength of the incident light only by ± 5 nm, leads to a $16\times$ drop in the amount of energy absorbed density by the MTJ, i.e. from 1 to 0.0625. Note that since the absorption profile is not uniform across the MTJ, to be able to switch the whole MTJ, we need to increase the power of the incident light by $\sim 90\%$ which may result in unwanted switching of a fraction of other bits in neighboring off-resonance cavities. Hence, it is crucial to conduct the study presented in section 2 to see if we can have a switching margin to guarantee the multiplexing performance of our device.

Based on the results of Fig. 5b and Fig. 3d, we implemented the design criteria for three cases of non-working, marginally-working, and unconditionally-working devices, respectively indicated by (i), (ii), and (iii) in Fig. 5b. The analysis results are shown in Fig. 6. Note that in this analysis, the absorption loss by the loaded cavities was considered $L_0 = 0.25$ at their resonance condition based on the numerical FDTD simulations. For the non-working device, i.e. case (i) where $U_{\text{th}} = 0.1\times U_{\text{sat}}$, which simply means that the maximum energy that we apply would be increased by 90% relative to the U_{min} , the result in Fig. 6a indicates that very high energies are required to switch the bits in this case which exceeds the required energy level for switching the bits in other cavities (see the red-dotted ellipse). In other words, due to the energy leakage, all other bits are switched-on inevitably in addition to the targeted bit. As for the case (ii) with $U_{\text{th}} = 0.4\times U_{\text{sat}}$, in contrast to the conditionally-working case in section 2, the minimum energy U_{min} is below the U_{max} limit for all cavities C_j for $j = 1$ to 8 (see Fig. 6b). However, the differences between U_{min} and the lowest of the U_{max} for all cavities across the whole network is very marginal which makes its multiplexing function susceptible to variations in the input pulse energy. That is why we called this case marginal. We then have the case where the device works unconditionally, i.e. the case (iii) with $U_{\text{th}} = 0.7\times U_{\text{sat}}$, the U_{min} limit is well below all the U_{max} limits across the network with a switching margin as large as 3.5 (see Fig. 6c). In this case, similar to the unconditionally-working case described in section 2, we have all desired events of switching with proper multiplexing function, thanks to its large switching margin.

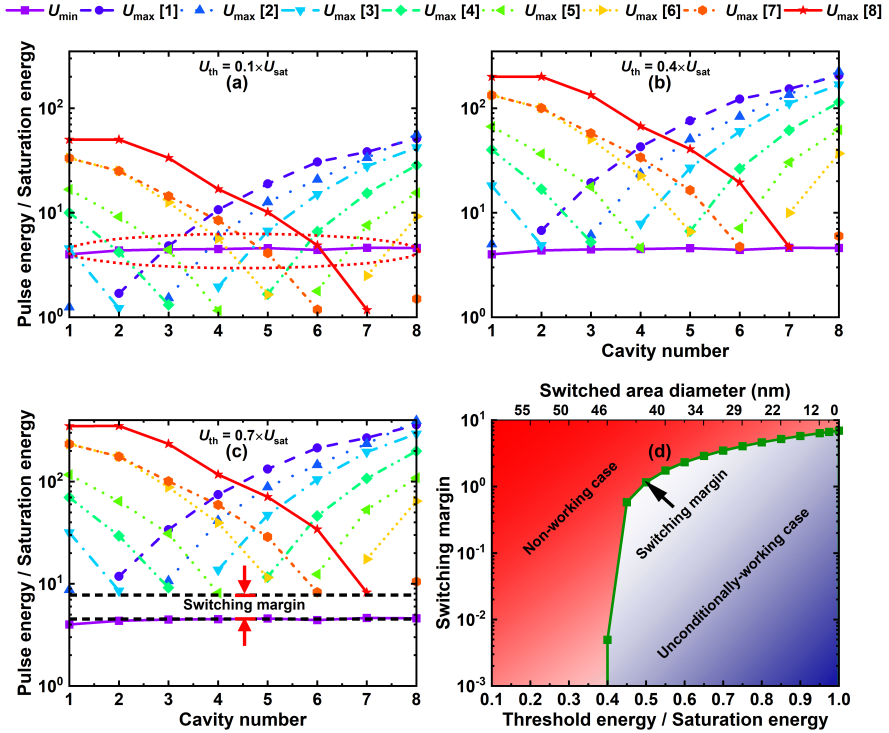


Fig. 6 All-optical switching (AOS) efficiency. Implementing the multiplexing criteria for the designed device in which the threshold energy U_{th} is: (a) $0.1 \times$ the saturation energy U_{sat} , (b) $0.4 \times U_{\text{sat}}$, and finally (c) $0.7 \times U_{\text{sat}}$. (d) Switching margin as a function the switched area diameter in nm and $U_{\text{th}} / U_{\text{sat}}$ ratio. The L_0 for the designed cavity is 0.25 at resonance.

In two cases of marginally-working and unconditionally-working devices discussed in the previous paragraph, depending on the ratio of the threshold energy to the saturation energy, i.e. $U_{\text{th}} / U_{\text{sat}}$, an area of the targeted MTJ with a unique diameter can be toggle-switched. For instance, in the cases of $U_{\text{th}} = 0.4 \times U_{\text{sat}}$ and $U_{\text{th}} = 0.7 \times U_{\text{sat}}$, areas of the MTJ with diameters of 46 nm and 32 nm get switched-on which are equal to the 77% and 53.3% of the MTJ surface area, respectively (see the values on the X axis of Fig. 5b corresponding to the cases of (ii) and (iii)). So, one can see there is a relation between the switching margin and both the $U_{\text{th}} / U_{\text{sat}}$ ratio and switched area diameter. Therefore, we provided an overview plot in Fig. 6d showing the dependency of the switching margin, the green symbol-line curve, on the above-mentioned parameters. According to this figure, for $U_{\text{th}}/U_{\text{sat}} \geq 0.4$, equivalent to switched area diameters of ≤ 46 nm, the switching event with proper multiplexing function can happen while its switching margin increases with increase in the

$U_{\text{th}}/U_{\text{sat}}$ ratio. It is worthwhile mentioning that considering the dynamics of domain walls and the size of the target MTJ, we can still have a single domain switching when the switched area is 53.3% of the MTJ surface area.

Overall, based on the combination of the numerical simulations and our proposed analytical study in section 2, we illustrated a device concept to enable magneto-photonic non-volatile multi-bits spintronic memory based on the WDM scheme with at least 8 bits in the telecommunication C-band.

4 Discussion

Integrating opto MTJs on photonic chips has been considered as an interesting option for hybrid integration of spintronics and photonics from the switching speed and energy perspectives [38, 50, 52]. To enable the realization of this concept, it is advantageous to design a platform to provide large scale integration of MTJs and parallel access for switching and reading at will. That is why in this work, we presented a device concept based on the near-field coupling WDM scheme in a PhC-based add/drop network, which is significantly advantageous in terms of the footprint and energy efficiency. Besides, our proposed device is completely monolithic, its simplicity of integration could potentially allow for easy incorporation of spintronic building blocks. It is noteworthy mentioning that we designed our device for IMOS, but the concept is generic and can be seamlessly transferred to other integrated photonic platforms, most notably SiPh, which has similar waveguide geometries and material indices of refraction as IMOS, and with a lower two-photon absorption.

It is important to note the characteristics of AOS. Much higher energy above AOS threshold leads to a multi-domain state or thermal demagnetization [32, 53, 54]. There is a fluence gap between AOS and the multi-domain state. This fluence gap diminishes as pulse duration increases [54]. During the AOS event, it is essential that the part in which the absorption is the least should be switched. At the same time, for the same pulse energy, no multi-domain state should be triggered at the part where the absorption is the most. Consequently, it is necessary to guarantee that this absorption in-homogeneity should lie within the fluence window, f_w , which is defined as the ratio between the threshold fluence of multi-domain state and AOS. As shown in Fig. 6, an in-homogeneity of $U_{\text{th}} = 0.4 \times U_{\text{sat}}$ is at the boundary to guarantee the functionalities of our designed building block. Thus, in this extreme case, the fluence window of $f_w > 2.5 (= 1/0.4)$ is at least necessary, imposing the longest pulse duration limit, reducing the effectiveness of photonic crystal cavity. As the in-homogeneity decreases, the necessary fluence window is less. Fortunately, as discussed, smaller MTJ devices are inherently less susceptible to homogeneity discrepancies, thus necessitating a reduced fluence window. This coincidence is aptly exemplified in Fig. 6, ultimately enhancing likewise our switching margin. Based on the bandwidth requirement of our designed device discussed in section 3, we found a pulse duration equal to/longer than 1 ps is necessary, as the pulse bandwidth needs to fit into the resonator bandwidth.

Recent experimental data [55] has demonstrated a fluence gap more than two at such a pulse duration which validates our design scenarios as discussed in Figs. 6b and 6c.

Our theoretical investigation detailed in section 2.2 also argued the benefit of decreasing the spectrum width of the cavity to increase the switching margin as well as to create the potential of fitting more cavities, i.e. more bits. Nevertheless, we note that care must be taken in this process. As the spectrum width narrows down, pulse duration needs to be increased accordingly, which reduces the tolerance for the above-mentioned multi-domain state. We therefore suggest to adopt AOS materials with longer maximum pulse duration, while at the operation pulse duration, the ratio between the threshold energy of thermal demagnetization and AOS needs to be enough substantial.

5 Conclusion

We have demonstrated an integrated hybrid photonic-spintronic device concept, enabling random AOS of 8 nanoscale MTJs coupled onto an IMOS platform. The device comprises of 8 PhC nanobeam cavities with different resonance wavelengths covering the telecommunication C-band, within a bandwidth of 35 nm, in each of which an MTJ is coupled. The cavities offered significant spatially-localized electric field enhancement thanks to the strong light-matter interaction which leads to substantial increase of the absorbed energy density in the coupled MTJs and consequent switching. We introduced an analytical approach as a general guideline for designing multi-bits spintronic memory based on add/drop networks working on the WDM scheme. Numerical FDTD results showed that our device can multiplex between the MTJs by de-tuning the wavelength of the incident light only by 5 nm, given the enhanced absorbed energy density in the coupled MTJs, thanks to PhC cavities. In this way, we can decisively and at the same time randomly switch any MTJ at will without unprecedented switching of any other MTJ in the network. We believe this device offers good prospects as a building block for developing an opto-spintronic memory and photonic buffer technology with possible potential in newly-emerged spintronic-based neuromorphic computing.

Acknowledgments. This work is part of the Gravitation programme “Research Centre for Integrated Nanophotonics”, which is financed by the Netherlands Organisation for Scientific Research (NWO). This project has also received funding from the European Union’s Horizon 2020 research and innovation programme under the Marie Skłodowska-Curie grant agreement No. 860060.

Declarations

The authors declare no competing interests.

References

- [1] Almeida, V.R., Barrios, C.A., Panepucci, R.R., Lipson, M.: All-optical control of light on a silicon chip. *Nature* **431**(7012), 1081–1084 (2004)
- [2] Levy, J.S., Gondarenko, A., Foster, M.A., Turner-Foster, A.C., Gaeta, A.L., Lipson, M.: Cmos-compatible multiple-wavelength oscillator for on-chip optical interconnects. *Nature photonics* **4**(1), 37–40 (2010)
- [3] Bogaerts, W., Pérez, D., Capmany, J., Miller, D.A., Poon, J., Englund, D., Morichetti, F., Melloni, A.: Programmable photonic circuits. *Nature* **586**(7828), 207–216 (2020)
- [4] Cheng, Z., Ríos, C., Pernice, W.H., Wright, C.D., Bhaskaran, H.: On-chip photonic synapse. *Science advances* **3**(9), 1700160 (2017)
- [5] Feldmann, J., Youngblood, N., Wright, C.D., Bhaskaran, H., Pernice, W.H.: All-optical spiking neurosynaptic networks with self-learning capabilities. *Nature* **569**(7755), 208–214 (2019)
- [6] Shastri, B.J., Tait, A.N., Ferreira de Lima, T., Pernice, W.H., Bhaskaran, H., Wright, C.D., Prucnal, P.R.: Photonics for artificial intelligence and neuromorphic computing. *Nature Photonics* **15**(2), 102–114 (2021)
- [7] Borkar, S.: Role of interconnects in the future of computing. *Journal of Lightwave Technology* **31**(24), 3927–3933 (2013)
- [8] Doerr, C.R.: Silicon photonic integration in telecommunications. *Frontiers in Physics* **3**, 37 (2015)
- [9] Pan, Z., Yu, C., Willner, A.E.: Optical performance monitoring for the next generation optical communication networks. *Optical Fiber Technology* **16**(1), 20–45 (2010)
- [10] Tucker, R.S., Ku, P.-C., Chang-Hasnain, C.J.: Slow-light optical buffers: capabilities and fundamental limitations. *Journal of lightwave technology* **23**(12), 4046 (2005)
- [11] Okawachi, Y., Foster, M.A., Sharping, J.E., Gaeta, A.L., Xu, Q., Lipson, M.: All-optical slow-light on a photonic chip. *Optics Express* **14**(6), 2317–2322 (2006)
- [12] Liu, L., Kumar, R., Huybrechts, K., Spuesens, T., Roelkens, G., Geluk, E.-J., De Vries, T., Regreny, P., Van Thourhout, D., Baets, R., *et al.*: An ultra-small, low-power, all-optical flip-flop memory on a silicon chip. *Nature Photonics* **4**(3), 182–187 (2010)
- [13] Fushimi, A., Tanabe, T.: All-optical logic gate operating with single

- wavelength. *Optics express* **22**(4), 4466–4479 (2014)
- [14] Benisty, H., Lourtioz, J.-M., Chelnokov, A., Combrie, S., Checoury, X.: Recent advances toward optical devices in semiconductor-based photonic crystals. *Proceedings of the IEEE* **94**(5), 997–1023 (2006)
- [15] Ríos, C., Stegmaier, M., Hosseini, P., Wang, D., Scherer, T., Wright, C.D., Bhaskaran, H., Pernice, W.H.: Integrated all-photonic non-volatile multi-level memory. *Nature photonics* **9**(11), 725–732 (2015)
- [16] O’Brien, J.L.: Optical quantum computing. *Science* **318**(5856), 1567–1570 (2007)
- [17] Fang, Z., Chen, R., Zheng, J., Khan, A.I., Neilson, K.M., Geiger, S.J., Callahan, D.M., Moebius, M.G., Saxena, A., Chen, M.E., *et al.*: Ultra-low-energy programmable non-volatile silicon photonics based on phase-change materials with graphene heaters. *Nature Nanotechnology* **17**(8), 842–848 (2022)
- [18] Zhang, H., Zhou, L., Lu, L., Xu, J., Wang, N., Hu, H., Rahman, B.A., Zhou, Z., Chen, J.: Miniature multilevel optical memristive switch using phase change material. *ACS Photonics* **6**(9), 2205–2212 (2019)
- [19] Zheng, J., Fang, Z., Wu, C., Zhu, S., Xu, P., Doylend, J.K., Deshmukh, S., Pop, E., Dunham, S., Li, M., *et al.*: Nonvolatile electrically reconfigurable integrated photonic switch enabled by a silicon pin diode heater. *Advanced Materials* **32**(31), 2001218 (2020)
- [20] Li, Y., Liu, F., Han, G., Chen, Q., Zhang, Y., Xie, X., Zhang, L., Lian, Y.: Design of an electric-driven nonvolatile low-energy-consumption phase change optical switch. *Nanotechnology* **32**(40), 405201 (2021)
- [21] Wuttig, M., Bhaskaran, H., Taubner, T.: Phase-change materials for non-volatile photonic applications. *Nature photonics* **11**(8), 465–476 (2017)
- [22] Zheng, J., Khanolkar, A., Xu, P., Colburn, S., Deshmukh, S., Myers, J., Frantz, J., Pop, E., Hendrickson, J., Doylend, J., *et al.*: Gst-on-silicon hybrid nanophotonic integrated circuits: a non-volatile quasi-continuously reprogrammable platform. *Optical Materials Express* **8**(6), 1551–1561 (2018)
- [23] Li, X., Youngblood, N., Cheng, Z., Carrillo, S.G.-C., Gemo, E., Pernice, W.H., Wright, C.D., Bhaskaran, H.: Experimental investigation of silicon and silicon nitride platforms for phase-change photonic in-memory computing. *Optica* **7**(3), 218–225 (2020)
- [24] Li, X., Youngblood, N., Ríos, C., Cheng, Z., Wright, C.D., Pernice, W.H.,

- Bhaskaran, H.: Fast and reliable storage using a 5 bit, nonvolatile photonic memory cell. *Optica* **6**(1), 1–6 (2019)
- [25] Feldmann, J., Youngblood, N., Li, X., Wright, C.D., Bhaskaran, H., Pernice, W.H.: Integrated 256 cell photonic phase-change memory with 512-bit capacity. *IEEE Journal of Selected Topics in Quantum Electronics* **26**(2), 1–7 (2019)
- [26] Wolf, S.A., Chtchelkanova, A.Y., Treger, D.M.: Spintronics—a retrospective and perspective. *IBM journal of research and development* **50**(1), 101–110 (2006)
- [27] Kimel, A.V., Kirilyuk, A., Rasing, T.: Femtosecond opto-magnetism: ultrafast laser manipulation of magnetic materials. *Laser & Photonics Reviews* **1**(3), 275–287 (2007)
- [28] Dieny, B., Prejbeanu, I.L., Garello, K., Gambardella, P., Freitas, P., Lehn-dorff, R., Raberg, W., Ebels, U., Demokritov, S.O., Akerman, J., Deac, A., Pirro, P., Adelmann, C., Anane, A., Chumak, A.V., Hirohata, A., Mangin, S., Valenzuela, S.O., Onbaşlı, M.C., d’Aquino, M., Prenat, G., Finocch-
chio, G., Lopez-Diaz, L., Chantrell, R., Chubykalo-Fesenko, O., Bortolotti, P.: Opportunities and challenges for spintronics in the microelectronics industry. *Nat. Electron.* **3**(8), 446–459 (2020)
- [29] Bhatti, S., Sbiaa, R., Hirohata, A., Ohno, H., Fukami, S., Piramanayagam, S.: Spintronics based random access memory: a review. *Materials Today* **20**(9), 530–548 (2017)
- [30] Alexey V.Kimel, M.L.: Writing magnetic memory with ultrashort light pulses. *Nat. Rev. Mater.* **4**, 189–200 (2019)
- [31] Ostler, T.A., Barker, J., Evans, R.F.L., Chantrell, R.W., Atxitia, U., Chubykalo-Fesenko, O., El Moussaoui, S., Le Guyader, L., Mengotti, E., Heyderman, L.J., Nolting, F., Tsukamoto, A., Itoh, A., Afanasiev, D., Ivanov, B.A., Kalashnikova, A.M., Vahaplar, K., Mentink, J., Kirilyuk, A., Rasing, T., Kimel, A.V.: Ultrafast heating as a sufficient stimulus for magnetization reversal in a ferrimagnet. *Nat. Commun.* **3**(1), 666 (2012)
- [32] Lalieu, M.L.M., Peeters, M.J.G., Haenen, S.R.R., Lavrijsen, R., Koopmans, B.: Deterministic all-optical switching of synthetic ferrimagnets using single femtosecond laser pulses. *Phys. Rev. B* **96**(22), 220411 (2017)
- [33] Li, P., Peeters, M.J.G., van Hees, Y.L.W., Lavrijsen, R., Koopmans, B.: Ultra-low energy threshold engineering for all-optical switching of magnetization in dielectric-coated Co/Gd based synthetic-ferrimagnet. *Appl. Phys. Lett.* **119**(25), 252402 (2021). <https://doi.org/10.1063/5.0077491>

- [34] Li, P., Kools, T.J., Koopmans, B., Lavrijsen, R.: Ultrafast racetrack based on compensated co/gd-based synthetic ferrimagnet with all-optical switching. *Advanced Electronic Materials* **9**(1), 2200613 (2023)
- [35] Becker, H., Krüchel, C.J., Thourhout, D.V., Heck, M.J.R.: Out-of-plane focusing grating couplers for silicon photonics integration with optical mram technology. *IEEE J. Sel. Top. Quantum Electron.* **26**(2), 1–8 (2020)
- [36] Pezeshki, H., Li, P., Lavrijsen, R., Van Der Tol, J.J., Koopmans, B.: Optical reading of nanoscale magnetic bits in an integrated photonic platform. *IEEE Journal of Quantum Electronics* (2022)
- [37] Pezeshki, H., Li, P., Lavrijsen, R., Heck, M., Bente, E., van der Tol, J., Koopmans, B.: Integrated hybrid plasmonic-photonic device for all-optical switching and reading of spintronic memory. *Physical Review Applied* **19**(5), 054036 (2023)
- [38] Wang, L., Houyi, C., Pingzhi, L., van Hees Youri L. W., Yang, L., Kaihua, C., Reinoud, L., Xiaoyang, L., Bert, K., Weisheng, Z.: Picosecond optospintronic tunnel junctions. *Proc. Natl. Acad. Sci.* **119**(24), 2204732119 (2022)
- [39] Pezeshki, H., Ahmadi, V.: Nanoscale effects on multichannel add/drop filter based on 2-d photonic crystal ring-resonator heterostructure. *Journal of Theoretical and Applied Physics* **6**, 1–6 (2012)
- [40] Pezeshki, H., Darvish, G.: Design of photonic crystal microcavity based optical switches using fano resonance effect. *Optik* **126**(23), 4202–4205 (2015)
- [41] Pezeshki, H., Darvish, G.: Design and simulation of photonic crystal based all-optical logic gate and modulator using infiltration. *Opt. Quantum Electron.* **48**(8), 1–15 (2016)
- [42] Lumerical Inc. <https://www.lumerical.com/products/fdtd/> (2021)
- [43] Bogaerts, W., Baets, R., Dumon, P., Wiaux, V., Beckx, S., Taillaert, D., Luyssaert, B., Van Campenhout, J., Bienstman, P., Van Thourhout, D.: Nanophotonic waveguides in silicon-on-insulator fabricated with CMOS technology. *J. Light. Technol.* **23**(1), 401–412 (2005)
- [44] Bogaerts, W., De Heyn, P., Van Vaerenbergh, T., De Vos, K., Kumar Selvaraja, S., Claes, T., Dumon, P., Bienstman, P., Van Thourhout, D., Baets, R.: Silicon microring resonators. *Laser Photonics Rev.* **6**(1), 47–73 (2012)

- [45] Subramanian, A., Neutens, P., Dhakal, A., Jansen, R., Claes, T., Rotenberg, X., Peyskens, F., Selvaraja, S., Helin, P., Du Bois, B., *et al.*: Low-loss singlemode PECVD silicon nitride photonic wire waveguides for 532–900 nm wavelength window fabricated within a CMOS pilot line. *IEEE Photon. J.* **5**(6), 2202809–2202809 (2013)
- [46] Blumenthal, D.J., Heideman, R., Geuzebroek, D., Leinse, A., Roeloffzen, C.: Silicon nitride in silicon photonics. *Proceedings of the IEEE* **106**(12), 2209–2231 (2018)
- [47] Mentink, J.H., Hellsvik, J., Afanasiev, D.V., Ivanov, B.A., Kirilyuk, A., Kimel, A.V., Eriksson, O., Katsnelson, M.I., Rasing, T.: Ultrafast spin dynamics in multisublattice magnets. *Phys. Rev. Lett.* **108**(5), 057202 (2012)
- [48] Li, P., van der Jagt, J.W., Beens, M., Hintermayr, J., Verheijen, M.A., Bruikman, R., Barcones, B., Juge, R., Lavrijsen, R., Ravelosona, D., *et al.*: Enhancing all-optical switching of magnetization by he ion irradiation. *Applied Physics Letters* **121**(17), 172404 (2022)
- [49] Li, P., Peeters, M.J., van Hees, Y.L., Lavrijsen, R., Koopmans, B.: Ultra-low energy threshold engineering for all-optical switching of magnetization in dielectric-coated Co/Gd based synthetic-ferrimagnet. *Appl. Phys. Lett.* **119**(25), 252402 (2021)
- [50] Chen, J.-Y., He, L., Wang, J.-P., Li, M.: All-optical switching of magnetic tunnel junctions with single subpicosecond laser pulses. *Phys. Rev. Appl.* **7**(2), 021001 (2017)
- [51] Pezeshki, H., Ahmadi, V.: All-optical bistable switching based on photonic crystal slab nanocavity using nonlinear kerr effect. *J. Mod. Opt.* **60**(2), 103–108 (2013)
- [52] Kim, S.K.: Fast and efficient switching with ferrimagnets. *Nat. Electron.* **3**(1), 18–19 (2020)
- [53] Stanciu, C.D., Hansteen, F., Kimel, A.V., Kirilyuk, A., Tsukamoto, A., Itoh, A., Rasing, T.: All-optical magnetic recording with circularly polarized light. *Phys. Rev. Lett.* **99**(4), 047601 (2007)
- [54] Wei, J., Zhang, B., Hehn, M., Zhang, W., Malinowski, G., Xu, Y., Zhao, W., Mangin, S.: All-optical helicity-independent switching state diagram in Gd-Fe-Co alloys. *Phys. Rev. Appl.* **15**(5), 054065 (2021)
- [55] Li, P., Kools, T.J., Pezeshki, H., Joosten, J.M.B.E., Li, J., Kalafat, D., Igarashi, J., Lavrijsen, R., Hohlfeld, J., Mangin, S., Malinowski, G., Koopmans, B.: Picosecond all-optical switching of co/gd based synthetic

ferrimagnet. To be published